Exploring the interactions of gliadins with model membranes: effect of confined geometry and interfaces.

Amélie Banc, B. Desbat, Denis Renard, Yves Popineau, Cécile Mangavel, Laurence Navailles

Exploring the Interactions of Gliadins with Model Membranes: Effect of Confined Geometry and Interfaces

Amélie Banc[†], Bernard Desbat[‡], Denis Renard[§], Yves Popineau[§], Cécile Mangavel[§], and Laurence Navailles*[†]

†*Centre de Recherche Paul Pascal, UPR 8641-CNRS, Avenue Albert Schweitzer, F-33600 Pessac,*
‡*Laboratoire de Chimie et Biologie des Membranes et Nanoobjets, UMR 5248-CNRS, Universite´ Bordeaux 1, ENITAB, 2 rue Robert Escarpit, F-33607 Pessac,*
§*UR1268 Biopolymères Interactions Assemblages, INRA, F-44300 Nantes.*

Mechanisms leading to the assembly of wheat storage proteins into proteins bodies within the endoplasmic reticulum of endosperm cells are unresolved today. In this work, physical chemistry parameters which could be involved in these processes were explored. In order to model the confined environment of proteins within the endoplasmic reticulum, the dynamic behavior of γ-gliadins inserted inside lyotropic lamellar phases was studied using FRAP experiments. The evolution of the diffusion coefficient as a function of the lamellar periodicity enabled to propose the hypothesis of an interaction between γ-gliadins and membranes. This interaction was further studied with the help of phospholipid Langmuir monolayers. γ- and ω-gliadins were injected under DMPC and DMPG monolayers and the 2D systems were studied by Brewter Angle Microscopy (BAM), Polarization Modulation Infrared Reflection-Absorption Spectroscopy (PM-IRRAS), and surface tension measurements. Results showed that both gliadins adsorbed under phospholipid monolayers, considered as biological membrane models, and formed micrometer-sized domains at equilibrium. However, their thicknesses, probed by reflectance measurements, were different: ω-gliadins aggregates displayed a constant thickness, consistent with a monolayer, while the thickness of γ-gliadins aggregates increased with the quantity of protein injected. These different behaviors could find some explanations in the difference of aminoacid sequence distribution: an alternate repeated – unrepeated domain within γ-gliadin sequence, while one unique repeated domain was present within ω-gliadin sequence. All these findings enabled to propose a model of gliadins self-assembly via a membrane interface and to highlight the predominant role of wheat prolamin repeated domain in the membrane interaction. In the biological context, these results would mean that the repeated domain could be considered as an anchor for the interaction with the endoplasmic reticulum membrane and a nucleus point for the formation and growth of protein bodies within endosperm cells.

Introduction

Wheat storage proteins (WSP), constituting gluten, are very important for various technological applications ranging from baking performances[1], to the elaboration of biomaterials[2], and the development of new drug delivery systems[3]. Moreover, as wheat is the world's largest crop, these storage proteins are the major source of dietary protein for human and livestock.

Most of WSP are classified as prolamins because of their high proportions of proline and glutamine. Despite their high proportion in polar glutamine residues, prolamins are poorly soluble in water. However they can be dissolved in water-alcohol mixtures or in low pH solutions[4]. WSP display a very extensive polymorphism, but they present a common feature which is the presence of repeated amino acid sequences in their primary structures. Prolamins are subdivided into two groups based on their ability to form polymeric systems by means of intermolecular disulfide bonds between protein subunits[5]. Gliadins are monomeric proteins, whereas glutenins are polymeric ones. Gliadins account for about half of the gluten proteins, and are subdivided into four types according to their electrophoretic mobility in acid-polyacrylamide gel electrophoresis, commonly denoted as α-, β-, γ-, and ω-gliadins. α-, β- and γ- gliadins have similar primary structures. They are composed of a short N-terminal domain, a repetitive domain which contains repeated motifs rich in proline, glutamine and phenylalanine, and a non-repetitive domain which includes all intramolecular disulphide bonds. Their primary structure indicates that the non-repetitive domain is more hydrophobic than the repetitive one, suggesting an amphiphilic feature of these gliadins. ω-gliadins principally consist of proline and glutamine residues, and are made up almost entirely of repeated domains without cysteines to form disulphide bonds[6]. ω-gliadins are globally more polar than α-, β- and γ-gliadins[7].

Table I Putative Sequences of γ_{46}-Gliadin and "Slow" ω-Gliadin

Putative sequence of γ_{46}-gliadin
NIQVDPSSQV QWLQQQLVPQ LQQPLSQQPQ QTFPQPQQTF PHQPQQQVPQ
PQQPQQPFLQ PQQPFPQQPQ QPFPQTQQPQ QPFPQQPQQP FPQTQQPQQP
FPQQPQQPFP QTQQPQQPFP QLQQPQQPFP QPQQQLPQPQ QPQQSFPQQQ
RPFIQPSLQQ QLNPCKNILL QQCKPASLVS SLWSIIWPQS DCQVMRQQCC
QQLAQIPQQL QCAAIHSVVH SIIMQQQQQQ QQQQGMHIFL PLSQQQQVGQ
GSLVQGQGII QPQQPAQLEA IRSLVLQTLP SMCNVYVPPE CSIMRAPFAS
IVAGIGGQ
308 Amino acid residues
Calculated MM: 35228
Measured MM: 35195
Theoretical pI: 10.10 net charge at pH7: +2.4

Putative sequence of "slow" ω-gliadin
ARELNPSNKE LQSPQQSFSH QQQPFPQQPY PQQPYPSQQP YPSQQPFPTP
QQQFPQQSQQ PFTQPQQPTP LQPQQPFPQQ PQQPQQPFPQ PQQPFPWQPQ
QPFPQTQQSF PLQPQQPFPQ QPQQPFPQPQ LPFPQQSEQV IPQQPQQPFP
LQPQQPFPQQ PQQPFPQPQQ PIPVQPQQSF PQQSQQSQQP FAQPQQLFPE
LQQPIPQQPQ QPFPLQPQQP FPQQPQQPFP QQPQQSFPQQ PQQPYPQQQQ
SFPQQPQQPF PQPQPQQPFP LRPQQPFPQQ PQQSQQSFLQ PQPQQPQQPS
ILQPQQPLPQ QPQQPFQQPQ QQLSQQPEQT ISQQPQQPFP QQPHQPQQPY
PQQQPYGSSL TSIGGQ
366 Amino acid residues
Calculated MM: 42752
Measured MM: 42749
Theoretical pI: 5.32 net charge at pH7: −2

In the biological context, WSP serve as amino acid source for germination, and are principally stored within protein from endoplasmic reticulum membranes, and may contain up to 80% of proteins[8]. The mechanisms leading to the formation of PB, and the organization of storage proteins inside the organelles, are not well understood today. An accumulation of proteins within the endoplasmic reticulum (ER), leading to the emergence of protein bodies in the cytoplasm, is suggested. However, due to the absence of a retention signal in the sequence of these proteins, the sequestration and the accumulation processes of proteins in the lumen of the ER are unexplained[9]. Today, mechanism involved was controlled by the intrinsic structure of proteins as well as by the ER environment. The strategy of this work was thus to study the behavior of model WSP in a confined environment similar to the ER, in order to identify key parameters of the accumulation process. Considering the high membrane surface in the ER, the interactions between WSP and membranes were more particularly studied. To our knowledge, the hypothesis of such interactions was scarcely studied. Kogan *et al*[14] revealed the interaction between a peptide corresponding to the repetitive domain of γ-zein (a maize storage protein) with soybean phosphatidylcholine liposomes. In the case of wheat, it was observed that total gliadins could modify mechanical properties of giant unilamellar vesicles membranes[15].

In our study, model WSP used were γ-gliadins and ω-gliadins. γ-gliadins are considered as an ancestral form of storage proteins, and were shown to be able to form alone PB in heterologous systems[9]. ω–gliadins were also used because their involvement in PB formation could be different due to their fully repetitive sequence. This bodies in developing grains, before their maturity. Protein bodies (PB) are micrometer-sized organelles emerging understanding the mechanisms involved in the unconventional protein traffic pathways which lead to PB formation, is a great challenge in plant biology[10]. Moreover, the organization of WSP in the biological context, as well as their composition, should be important for wheat grain quality. The aim of the study is to elucidate physical chemical parameters involved in the organization of WSP in the cellular context.

The formation of natural-like PB with prolamins expressed in different heterologous systems[11,12,13] suggested that the assumption is supported by the different surface properties of γ- and ω-gliadins at the air-water interface[16]. Furthermore, ω-gliadins should be considered as a model of the repetitive domain of γ-gliadins. In a first part, lyotropic lamellar phases, consisting of stacks of surfactant bilayers separated by aqueous layers, were used as an ER model environment for gliadins. This 3D approach enabled us to study both the confinement effect on the proteins assembly, and to suggest an interaction between gliadins and membranes. However, the results obtained with this approach being not sufficient to firmly conclude on the gliadin-membrane interaction, in a second part, a 2D approach was carried out to look at the protein behavior at the water lipid interface. In this case, 1,2-Dimyristoyl-*sn*-Glycero-3-Phosphocholine (DMPC) and 1,2-Dimyristoyl-*sn*-Glycero-3-[Phospho-rac-(1-glycerol)] (DMPG) monolayers were used as ER model membranes. DMPC was chosen as it represents the major phospholipid contained in plant ER membranes[17], while DMPG was selected in order to study the effect of negative charges generally observed in biological membranes.

Experimental methods

1/ 3D approach: lyotropic lamellar phases system

Samples. γ- and ω-gliadins were purified according to Banc et al[16] procedure. The gliadin components used in this work were not fully sequenced. However it is possible to propose putative sequences (table 1) based on their measured molecular masses, partial sequences and other physicochemical properties with reference to literature[18,19,20, 21,22]. γ-gliadin was labeled with tetramethylrhodamine isothiocyanate (TRITC) according to a new procedure adapted for this protein which is not soluble in alkaline aqueous solutions. Briefly, the freeze-dried γ-gliadin was dissolved at 10 mg/ml in an ethanol-bicarbonate buffer (0.1 M, pH 9) mixture 45:55 (v/v) and incubated for 7 hours, at 50°C, with a TRITC solution at 10 mg/ml in DMSO. The molar ratio of TRITC to γ-gliadin in the initial reaction solution was 10. After reaction, the excess reagent was removed by extensive dialysis against a water-ethanol (45:55) solution, and the final molar ratio of TRITC to γ-gliadin, determined by UV spectroscopy, was 1.

The lamellar phase system was spontaneously formed with the non-ionic n-pentaethyleneglycol monododecylether surfactant $C_{12}E_5$ (Nikko Ltd), hexanol and water[23,24]. The hexanol/$C_{12}E_5$ weight ratio used was 0.29, and the water content was varied from 40 to 90 wt%. This range of aqueous fractions enabled to obtain monophasic smectic structures with repeat distances d ranging from 5 to 18 nm. Three different probes were mixed with the lyotropic lamellar formulations at constant concentration (0.08% (w/w)): The rhodamine-labeled γ-gliadin (γ-gliadin-TRITC), the rhodamine dye TRITC (mixed isomers, purchased from Aldrich) and the hydrophobic probe, rhodamine 1,2 dihexadecanoyl-sn-glycero-3-phosphoethanolamine (DHPE-TRITC, purchased from Invitrogen – Molecular Probes). After mixing, samples were let several days to reach equilibrium.

X-ray scattering. Small angle x-ray scattering experiments (Nanostar, Bruker) were performed in order to describe the host phase nature and to measure the lamellar spacing (d) of lamellar phase systems. Samples prepared with various water contents display various water layer thicknesses (d_w). The quantity d_w was deduced from the swelling behavior established using x-ray experiments as follows: the stacking period d of the lamellar phase was first obtained from the value q_{max} of the first order Bragg peak as $d = 2\pi/q_{max}$. Repeating the measurement for different water concentrations, the bilayer thickness δ was extracted from the swelling law $d = \delta/\varphi_m$, with φ_m the membrane volume fraction. The water layer thickness was finally deduced using the relation $d_w = d-\delta$.

Optical microscopy. Polarized light and fluorescence microscopy observations were done on a Leica SP2 confocal laser scanning microscope. For observations, flat capillaries (thickness e = 50 µm) were filled with the lamellar phase samples and sealed with a UV-curing adhesive (Norland Optical Adhesive 81).

*Diffusion coefficients determination using FRAP measurements.*FRAP measurements were performed using a confocal laser scanning microscope (CLSM) that gives high spatial resolution[25] and allows surgical bleaching. In order to measure the translational diffusion coefficient parallel to the layers ($D_\perp$, i.e. perpendicular to the optical axis), homeotropically oriented lamellar phases were used. In flat capillaries, the lamellar phase naturally adopted homeotropic anchoring (stacking axis perpendicular to the walls) and well oriented monodomains were thus obtained. The homeotropic orientation was checked using the optical polarized light microscopy technique, so that the laser beam was parallel to the normal of the layers. The bleaching and imaging were performed on a Leica SP2 confocal microscope with an oil immersion x63 objective lens (numerical aperture 1.4). A spot area of nearly 2 µm in radius was bleached during a time τ (in the range 1 to 10 s, depending on the sample). The image acquisition was made by scanning the field with a confocal photomultiplier (acquisition time of a few seconds) after a time t (1.635 s) had elapsed.

Analysis of data was performed according to the Moreau et al[26] method. In a first approximation, the lateral width of the laser beam spot was neglected. Secondly the permeation through the bilayers was considered to be so small that the diffusion coefficient for motions in the direction parallel to the optical axis ($D_{//}$) was assumed negligible compared to the translational diffusion ($D_\perp$) for species diffusing between nanometered-separated membranes. As a consequence, the concentration of bleached dyes c(r, t) versus space and time, initially non-zero only within the point-like laser spot, is found by integrating Fick's law in the 2D-space perpendicular to the optical axis, which leads to:

$$c(r,t) = \frac{c_0}{4\pi D_\perp t}\exp\left[-\frac{r^2}{4D_\perp t}\right] \quad (1)$$

when the bleaching duration was extremely short. In eq. (1), r is the distance from the center of the bleaching point, t the time, $D_\perp$ the diffusion coefficient in the layer plane, and c_0 a normalization constant depending mainly on dye concentration, power of the bleaching radiation, etc.

For the sake of simplicity, the depletion in fluorescence intensity at time t after a photo bleaching of finite duration τ is represented as the superimposition of time-translated expressions similar to eq. (1), namely:

$$I(r,t,\tau) = \int_0^\tau \frac{I_0}{t-\tau_1}\exp\left[-\frac{r^2}{4D_\perp(t-\tau_1)}\right]d\tau \quad (2)$$

with, $t > \tau$, and I_0 a normalization constant. Using this scheme, the fluorescence intensity could therefore be described by the equation:

$$I(r,t,\tau) = I_0\left(E_1\left[\frac{r^2}{4D_\perp t}\right] - E_1\left[\frac{r^2}{4D_\perp(t-\tau)}\right]\right) \quad (3)$$

with E_1 the exponential integral function of order 1. The diffusion coefficient $D_\perp$ was deduced from the recorded images by a numerical fitting using eq. (3), with only two fitting parameters, namely I_0 as an arbitrary intensity scale and $\sigma^2 \equiv 4D_\perp t$, since the bleaching duration τ was known.

2/ 2D approach: Langmuir films system

*Materials.*Experiments were done in a circular Teflon® trough 51 mm radius, filled with 8 mL of subphase. The subphase was constituted of a 50 mM pH 7.2 phosphate buffer previously filtered through a glass microfibre filter (GF/F, Whatman). The water used was purified from a milliQ system (Millipore, Molsheim, France) with a nominal resistivity of 18.2 MΩ.cm. Phospholipids monolayers were prepared with DMPC or DMPG purchased from Avanti Polar Lipids. Phospholipids were previously dissolved in chloroform (for DMPC), or chloroform:ethanol 4:1 (v/v) (for DMPG) at 0.5 mg/ml, and spread at the air-water interface using a Hamilton microsyringe according to the Langmuir method. The volume injected was adjusted in order to obtain the required monolayer pressure. Proteins used were γ-gliadins and ω-gliadins purified according to the Banc et al procedure[16]. Freeze-dried proteins were dissolved in a 48:52 (v/v) water:ethanol mixture at a concentration C = 1 mg/mL, and filtered through a 0.45 µm porosity filter (Millipore). After an equilibration time of the phospholipid monolayer, protein solutions were injected into the subphase using a Hamilton microsyringe. The surface pressure (π) was monitored by a Wilhelmy surface balance using a filter paper plate (Whatman).

*Brewster Angle Microscopy.*The surfaces of the films were observed using the Brewster angle microscope BAM2 plus (NFT, Göttingen, Germany) equipped with a frequency doubled Nd:YAG laser with a wavelength of 532 nm and a charge-coupled device (CCD) camera with a x10 magnification lens. The exposure time (ET), depending on the image luminosity, was adjusted from 20 to 0.5 ms to avoid saturation of the camera.The spatial lateral resolution of the Brewster angle microscope was 2 μm, and the image size was 400 x 650 μm². The BAM images were coded in grey level. To determine the reflectance of layers at the surface, the calibration procedure of the BAM software was used to determine the linear function between the reflectance and the grey level. This function was established by comparison between the experimental curve of the grey level as a function of the incidence angle and the Fresnel curve (curve of the reflectance as a function of the incidence angle) that can be fitted by a parabola around the Brewster angle minimum.

*PM-IRRAS. S*pectra were recorded on a Nicolet 870 Fourier transform infrared (FT-IR) spectrometer by co-addition of 600 scans at a resolution of 8 cm^{-1}. The details of the optical setup, the experimental procedure, and the two-channel processing of the detected intensity have been already described[27]. PM-IRRAS is a technique sensitive to the orientation of the transition moment at the water surface, and hence the molecular groups themselves. Briefly, the surface selection rule indicates positive bands for transition moment lying in the surface plane whereas negative bands are attributed to transition moments perpendicular to the surface. For an intermediate orientation of the transition dipole moment, the two contributions are competing and the absorption band vanishes when the transition dipole moment is tilted at 39° from the surface normal of the water subphase.

PM-IRRAS device allows obtaining of the differential reflectivity spectrum:

$$\Delta R/R = [(Rp-Rs)/(Rp+Rs)].J_2 \quad (4)$$

with Rp the p-polarized reflectance, Rs the s-polarized reflectance and J_2 the Bessel function.

To remove the contribution of the subphase absorption and the dependence on the Bessel function, the film spectra were divided by that of the subphase. The water vapor contribution on each film spectrum was removed by subtraction of water vapor spectrum.

Results

1/ 3D approach: lamellar phase system

Structural characterization. In order to study the behavior of model gliadins inside a membrane confined environment, lyotropic lamellar phases were formulated with labeled γ-gliadins. Hydrophilic and hydrophobic model probes were also prepared in the lamellar system to support the analysis.

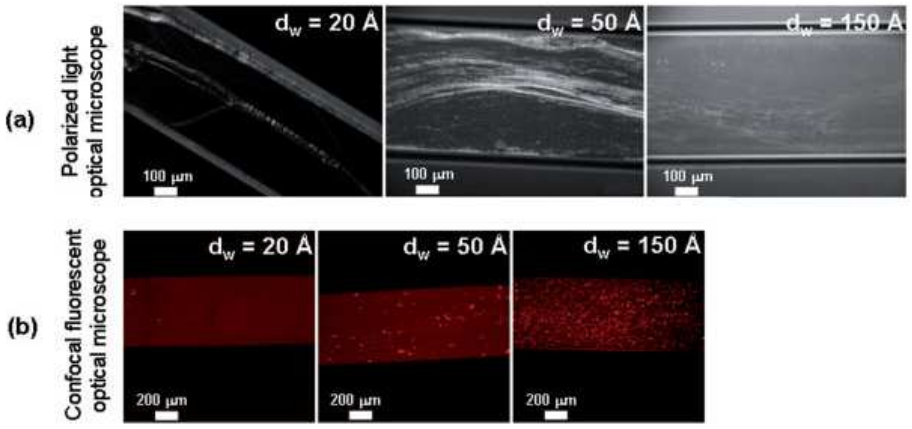

Figure 1. Images obtained using optical microscopes for the $C_{12}E_5$/Hexanol/water/γ-gliadin-TRITC system for three different water layer thicknesses (d_w). (a) Polarized light microscope and (b) Confocal fluorescent optical microscope.

Firstly, a characterization of the samples was performed to determine whether gliadins were inserted inside the lamellar phase or notFigure 1 displays microscopic observations of gliadin doped lamellar systems. The typical texture of defects of the lamellar structure[28] (oily streaks) appears using polarized light microscopy (Fig. 1a). The fluorescence intensity is homogeneous in homeotropic domains (Fig. 1b) when the membranes are parallel to the glass plates (*i.e.* the normal of the layer is parallel to the optical axes), and bright fluorescent spots are observed in the vicinity of the lamellar phase grain boundaries. These observations indicate a biphasic system of gliadins inserted inside the lamellar phase and aggregated gliadins outside the lamellar phase. The protein should be partially excluded from the lamellar phase so that the texture looses its homogeneity. This phenomenon is more pronounced in diluted systems. For the hydrophilic (TRITC) and hydrophobic (DHPE-TRITC) probes, a monophasic doped lamellar phase with the probe totally inserted inside the lamellar phase is always characterized.

The lamellar structure of doped samples was also checked by x-ray diffraction experiments. Figure 2 displays typical x-ray diffraction results obtained for lamellar systems formulated with γ-gliadin. Bragg peaks observed in Fig. 2a are consistent with the lamellar structure of the host phase. An intensity increase of the small angle scattering with dilution of the systems is also observed. Though not investigated in details, it may be correlated to the presence of large protein aggregates between lamellar phase grain boundaries observed by fluorescence microscopy. Fig. 2b compares the swelling law d vs $1/\varphi_m$ for the gliadin doped lamellar system and the undoped system previously studied by Freyssingeas et *al*[24]. The membrane thickness δ is found to be equal to 2.9 and 3.0 nm for the undoped and doped system, respectively. It turns out that the stacking periods are not significantly modified after addition of either protein (Fig. 2b) or probes (data not shown). The most important result is that gliadins may be inserted inside the lamellar phase for a large range of dilutions.

Dynamic inside the lamellar phases. The dynamic of the γ-gliadins inserted into lyotropic lamellar phases with various water contents was studied by FRAP experiments. As the image analysis is based on the Fick's law and equation (3), the Brownian dynamic of the different labeled molecules inside lamellar systems was checked measuring the parameter σ^2 as a function of time: The Gaussian broadening should be a simple linear function of the elapsed time t. Figure 3 shows the evolution of σ^2 versus time for the γ-gliadin-TRITC protein, TRITC and DHPE-TRITC probes inserted in the $C_{12}E_5$/Hexanol system with a water layer thickness (d_w) equal to 8 nm. From the observed linear behavior, unambiguous values for the diffusion coefficient could be deduced with our FRAP analysis method. Using FRAP experiments, the diffusion coefficient D⊥ of each probe as a function of the water layer thickness d_w of the $C_{12}E_5$/Hexanol/Water lamellar phase was measured.

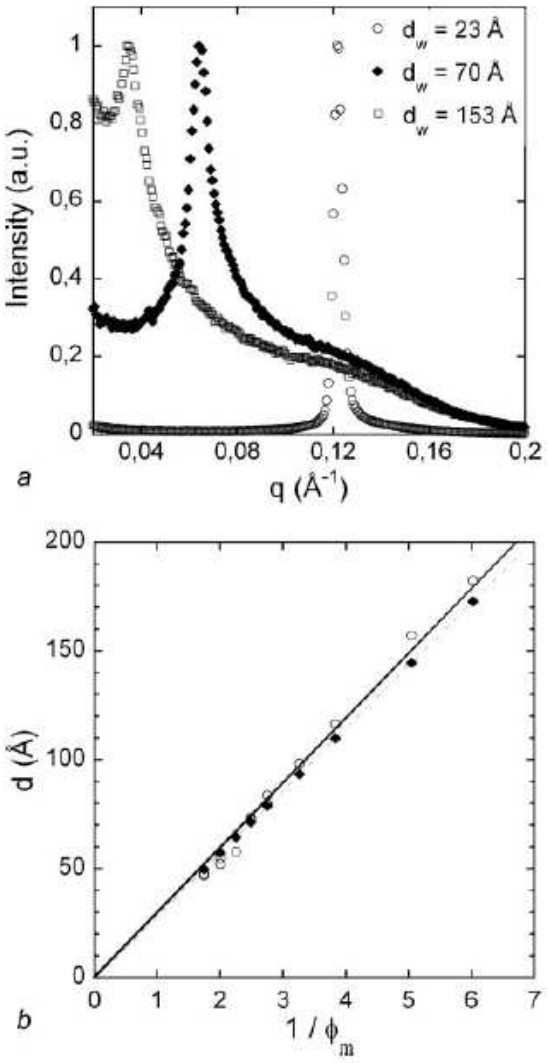

Figure 2. X-rays scattering experiments of γ-gliadins doped lamellar phases. (a) Bragg peaks of the γ-gliadin-TRITC protein inside the $C_{12}E_5$/Hexanol/water lamellar system for three different water layer thicknesses (d_w). (b) Evolution of the d-spacing as a function of the water content. Empty circles correspond to the protein doped lamellar phase and filled diamonds correspond to the same lamellar phase without proteins (Freyssingeas *et al*[19] data). The solid lines correspond to a linear fit using $d = \delta/\phi m$.

For the TRITC dye, the molecules should be encapsulated inside the water layer of the lamellar structure[26]. Despite the large error bars, it can be observed that at large d_w, the D⊥ values asymptotically approach 120 x 10^{-12} m^2/s; at lower d_w, the diffusion coefficient D⊥ significantly and steadily decreases; and a quasi-plateau, where D⊥ exhibits little variations with d_w, is reached for $d_w < 4.7$ nm (vertical full line in Fig. 4). The first (dilute) regime can be qualitatively explained by Faxén's model[29] for the 2D self-diffusion of a colloidal particle symmetrically confined between two rigid walls. According to this model, at high dw values the translational diffusion coefficient of the

diffusing object D⊥ tends towards the 3D free-diffusion coefficient value.

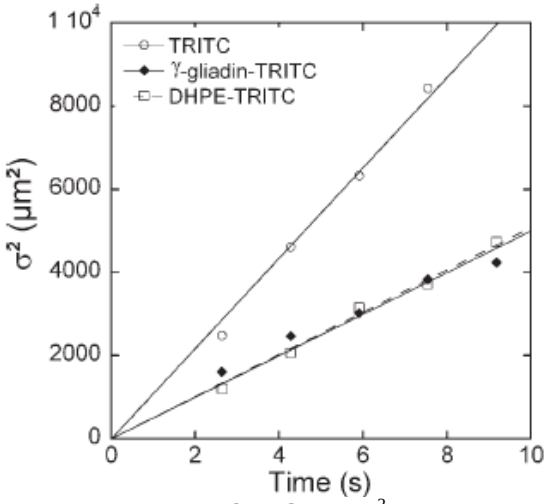

Figure 3. Gaussian broadening σ^2 versus time resulting from fits according to equation (3). The lines correspond to simple linear fits; $C_{12}E_5$ / Hexanol / water / TRITC system (empty circles), $C_{12}E_5$ / Hexanol / water / γ-gliadin-TRITC system (filled diamonds), $C_{12}E_5$ / Hexanol / water / DHPE-TRITC system (empty squares).

The second (concentrated or confined) regime, when the self-diffusion coefficient remains nearly constant for small membrane separations, was explained by the confinement (d_w < particle diameter) of particles between fluid membranes[26]. According to the authors, the limit between the two regimes is thus directly correlated to the diameter of the particle. It is interesting to note that the transition in our system apparently occurs for a d_w value (4.7 nm, vertical full line in Fig. 4) larger than the expected hydrodynamic diameter of the TRITC dye[30,31,32] (ca. 1 nm). At the same time, the diffusion coefficient for large d_w values is close to 120 x 10^{-12} m^2/s. This asymptotic value is much lower than the 3D free-diffusion coefficient D_0 (ca. 425 x 10^{-12} m^2/s) of TRITC calculated using the Stokes-Einstein equation (in water at 20°C). This equation relates the free diffusion coefficient of a hard sphere in a Newtonian fluid to the hydrodynamic radius, in the colloidal range in which the sphere is subject to Brownian motion:

$$D_0 = \frac{k_B T}{\zeta} = \frac{k_B T}{6\pi\eta_0 R_H} \qquad (5)$$

where k_B is the Boltzmann constant, T the temperature, ζ the drag coefficient η_0 the viscosity of the fluid and R_H the hydrodynamic radius. With D⊥ = 120 x 10^{-12} m^2/s, R_H calculated from equation 5 is 1.8 nm and should give a transition between the dilute and confined regimes for $d_w = 2R_H$ = 3.6 nm, a value consistently close to the d_w value (ca. 4.7 nm) measured for the TRITC dye encapsulated inside the lamellar phase. Taking into account the hydrodynamic radius R_H for the rhodamine dye (ca. 0.5 nm), it is therefore assumed that TRITC is present in an aggregated form inside the aqueous layer of the lamellar phase. The TRITC aggregation occurring in water, and being self-consistent with the chemical structure of the fluorophore, could also explain the large error bars obtained for diffusion coefficient from FRAP measurements.

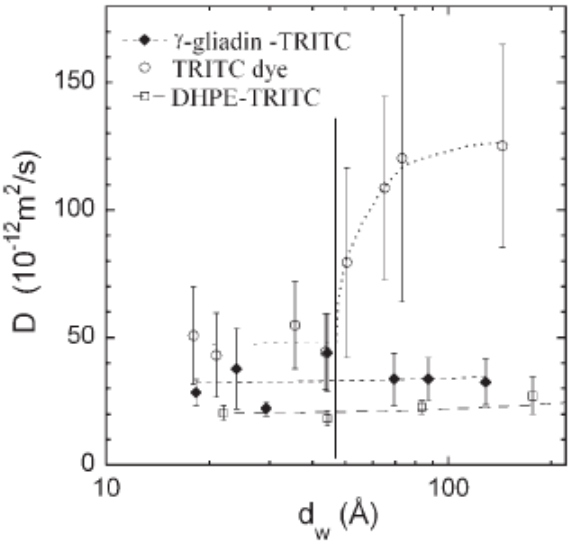

Figure 4. Diffusion coefficients D⊥ derived from FRAP experiments as a function of the water layer thickness d_w for three different doped $C_{12}E_5$/hexanol/water lamellar phases: free TRITC (empty circles), the γ-gliadin-TRITC (filled diamonds) and the DHPE-TRITC (empty squares). Vertical solid line drawn correspond to d_w = 4.7 nm.

For the DHPE-TRITC probe, the diffusion coefficient is mostly independent on swelling (Fig. 4, empty squares). The values are small (ca. 20 x 10^{-12} m^2/s) and do not vary with the confinement, behavior in agreement with amphiphilic probes diffusing along the bilayers. Interestingly, the same behavior is observed for the γ-gliadin-TRITC protein (Fig. 4, filled diamonds) encapsulated inside the $C_{12}E_5$/Hexanol/water lamellar phase. The diffusion coefficient value does not vary with d_w, and is equal to 30 x 10^{-12} m^2/s, a small value again. This invariance of the diffusion coefficient clearly indicates that γ-gliadin do not freely diffuse in the water layer of the lamellar structure. Either the proteins are in interaction with the bilayers, or they form large objects soluble in the aqueous medium which remain geometrically confined by adjacent bilayers in the whole range of d_w studied. In order to confirm and decipher a potential membrane-gliadin interaction, a complementary 2D approach was performed using different kinds of gliadins (γ- and ω-gliadins) and phospholipids (DMPC and DMPG).

2/ Langmuir films

Interfacial pressure 2D experiments were carried out using DMPC or DMPG monolayers at the air-water interface, as model membranes. Figure 5 displays the interfacial pressure evolution as function of time with the injection of

γ-gliadin solution under DMPC monolayers. When the phospholipid monolayer has an initial pressure of 20 mN/m, the γ-gliadin injection induces an abrupt increase of the interfacial pressure followed by stabilization at about 25 mN/m.

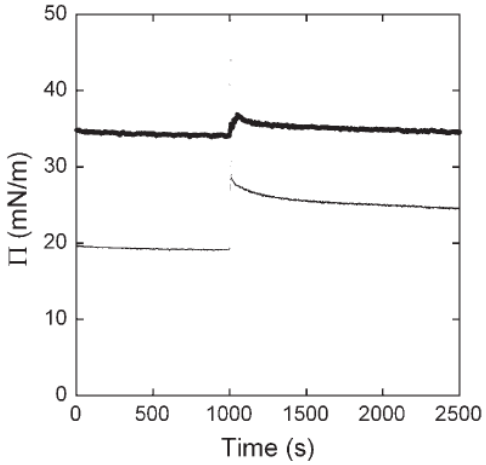

Figure 5. Evolution of the interfacial pressure Π (mN/m) as a function of time (s) with the injection of γ-gliadin (arrow) under DMPC monolayers at 20 mN/m (thin curve) and 35 mN/m (thick curve).

This increase of pressure can be ascribed to an insertion of gliadins inside the monolayer. When the DMPC monolayer has an initial pressure of 35 mN/m, even if a perturbation is firstly observed, the surface pressure is finally unmodified after a short equilibration time. At this higher pressure, γ-gliadins can not penetrate into the DMPC monolayer. The same behavior was observed with the DMPG monolayer. Keller *et al*[33] previously found that a complex gliadin fraction could not insert into lipid or emulsifier monolayers above a critical surface pressure. The gliadin insertion into DMPC or DMPG monolayers depends on interfacial pressure, as observed for numerous proteins[34, 35, 36]. In some cases, however the peptides expelled from the lipid monolayer remained adsorbed at the monolayer[36]. Because the biological membrane pressure is considered ranged from 25 to 35 mN/m[37], it can be supposed that γ-gliadins do not insert into biological membranes. In this range of surface pressures, ω-gliadins exhibit the same behavior as γ-gliadins. Only the system with a 35 mN/m initial pressure was further characterized because our study is related to the behavior of gliadins in the ER lumen.

BAM measurements. The effect of the injection of gliadins under DMPC monolayers was observed by Brewster Angle Microscopy. At 35 mN/m, DMPC monolayer displays a homogeneous aspect, with constant grey level (data not shown). After the injection of gliadins under the monolayer, appearances and disappearances of luminous dots, like blinking, was observed. As the reflectivity intensity observed by BAM is correlated to the refractive index and the thickness of the interfacial film, this phenomenon can be attributed to adsorption-desorption cycles of gliadins under the monolayer.

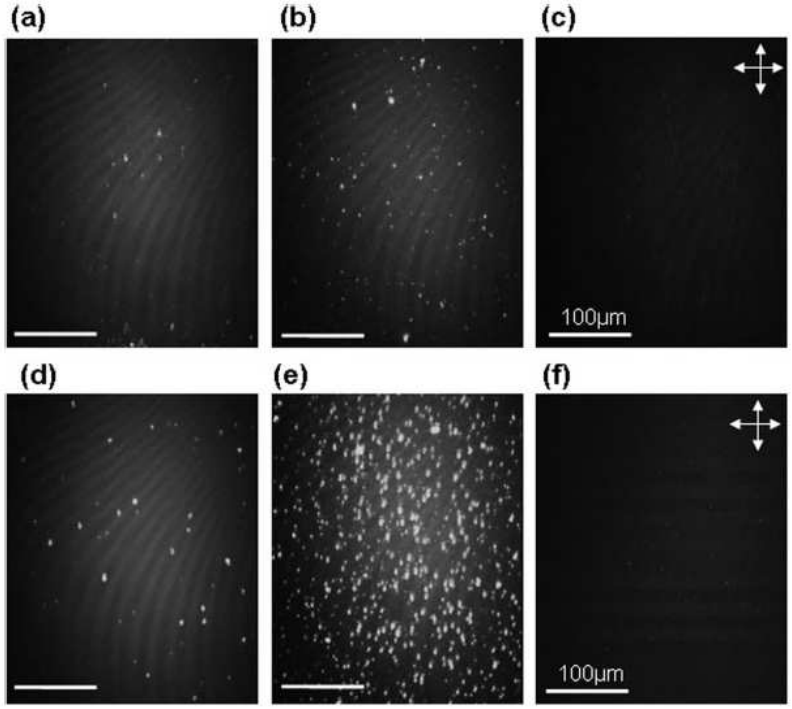

Figure 6. Brewster angle microscopy images of gliadins injected under a DMPC monolayer at Π = 35 mN/m. (a) 10µg ω-gliadin injected (b) 100µg ω-gliadin injected (c) 100µg ω-gliadin injected, observed between crossed polariser and analyser (d) 10µg γ-gliadin injected (e) 100µg γ-gliadin injected (f) 100µg γ-gliadin injected, observed between crossed polariser and analyser (Exposure Time= 1/50s).

After an equilibration time, the stabilized system displays bright dots on a field which has the same grey level as the pure DMPC monolayer (Fig. 6). Considering that the interfacial pressure is unchanged with the injection of gliadins, luminous dots can be ascribed to the gliadin adsorption under the phospholipidic monolayer. Moreover, the observation of the stabilized system by BAM with crossed polarizer and analyzer shows a dark picture (Fig. 6 c,f). This observation means that gliadin dots would be flat and smooth, because rough aggregates would induce scattering and depolarization of the incident light. Figure 6 (a,b,d,e) presents BAM pictures obtained after the injection of different quantities of γ- and ω-gliadins under the monolayer. In all cases, the diameter of bright dots is limited to few microns and it appears impossible to form a homogeneous protein film under the phospholipidic monolayer whereas such a film was formed with the same quantity of gliadin injected at the air-water interface[16]. For low protein quantities injected, both γ- and ω-gliadin systems present similar pictures, characterized by luminous dots with a micrometric radius. For higher gliadin quantities injected, γ-gliadin-DMPC monolayer system displays more numerous larger and brighter dots than ω-gliadin-DMPC monolayer system. The local reflectance intensity of the dots as a function of the injected gliadin quantity, and the reflectance - thickness relationship are plotted in Fig.7. The reflectance-thickness relationship is based on Fresnel equations and values were calculated by a software developed by Buffeteau et al[38]. The plot shows a periodical function indicating several thicknesses values for one reflectance value (Fig. 7b). The reflectance of γ-gliadin dots increases with the quantity of gliadin injected, whereas the reflectance of ω-gliadin dots is constant (Fig. 7a). The increase of reflectivity with the addition of γ-gliadins has to be attributed to an increase of thickness, rather than a decrease in thickness. In the thickness range presented, there are two regions in the periodical function where the reflectivity increases with the thickness. Considering a progressive thickness growth, to reach the high thicknesses regions, the reflectivity should have first increased then decreased. This behavior was not encountered in our study. Moreover, the reflectance values measured in the γ-gliadin system, ranging from 0 to 3.10^{-4}, are very low compared to the global reflectance range (ranging from 0 to $2.5.10^{-3}$). These reflectance values suggest very thin objects. The thickness values were estimated thanks to the following equation[39], which establishes a relationship between the reflectance and the square of the thickness, for a thin, single-layered interfacial film:

$$R = \frac{I_R}{I_0} = \left(\pi \frac{d}{\lambda}\right)^2 \frac{\left(n_1^2 - n_2^2 - 1 + \frac{n_2^2}{n_1^2}\right)^2}{1 + n_2^2} \quad (6)$$

where I_0 and I_R are the incident and the reflected intensity, n_1, n_2 the refractive indices of the film (1) and the subphase (2), λ the wavelength of the incident light and d the thickness of the film. Parameters used where λ = 532 nm, n_2 = 1.333 and n_1 = 1.47. The n_1 value is chosen as the refractive index of biological materials is known to be comprised between 1.43 and 1.47[39], and the protein-lipid monolayer assembly is considered to be continuous. As a consequence, the n_1 refractive index value is an estimation which implies an uncertainty in the thickness value calculated. The DMPC monolayer thickness value thus obtained is 2.2 nm, a value in agreement with those found in literature[40]. The average thicknesses corresponding to the dots reflectance are comprised between 8 and 20 nm in the presence of γ-gliadins and about 6 nm in the presence of ω-gliadins. Considering the DMPC monolayer thickness, the γ-gliadin aggregates thickness grows approximately from 6 to 18 nm with the addition of proteins, whereas the ω-gliadin aggregates thickness is constant and approximately equals to 4 nm. With low quantities of γ- and ω-gliadins injected, the aggregates thicknesses suggest gliadin monolayers adsorbed under the DMPC monolayer.

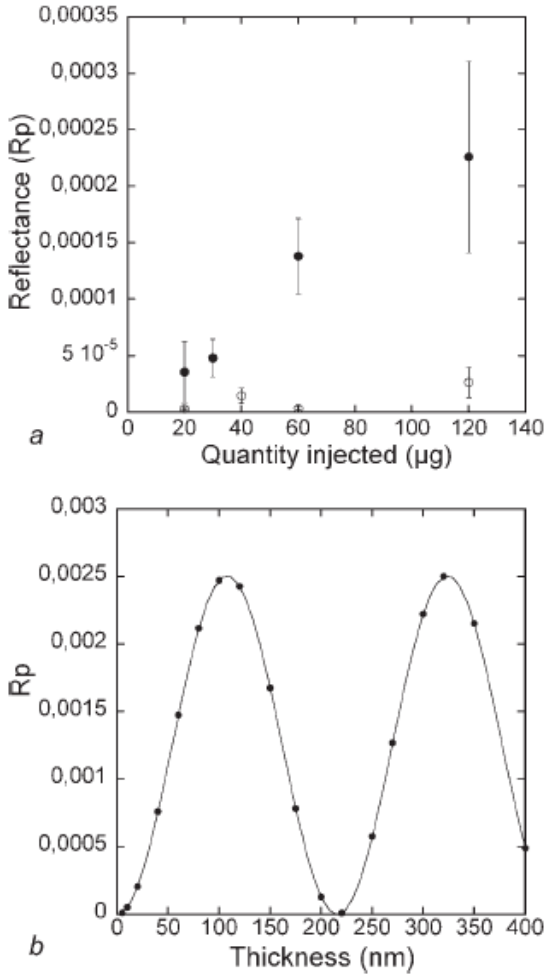

Figure 7. (a) Evolution of the local reflectance of aggregates (luminous dots) versus gliadin quantity injected. Filled dots: γ-gliadin, unfilled dots: ω-gliadin. (b) Brewster Angle Microscopy model of reflectance versus thickness (incidence wavelengh λ = 532 nm, incidence angle θ = 53.17°, film refractive index n=1.47).

With high quantities of γ-gliadins injected, but not ω-gliadins, the calculated thickness suggests a multilayer structure of the protein aggregates. Brewster Angle microscopic observations of systems made with DMPG monolayers were also carried out. Observations were qualitatively the same as those performed using DMPC monolayers. It was also observed the formation of flat, circular, micrometric gliadin aggregates under the lipidic monolayer, whose reflectivity depended on the quantity of protein injected in the γ-gliadin case only.

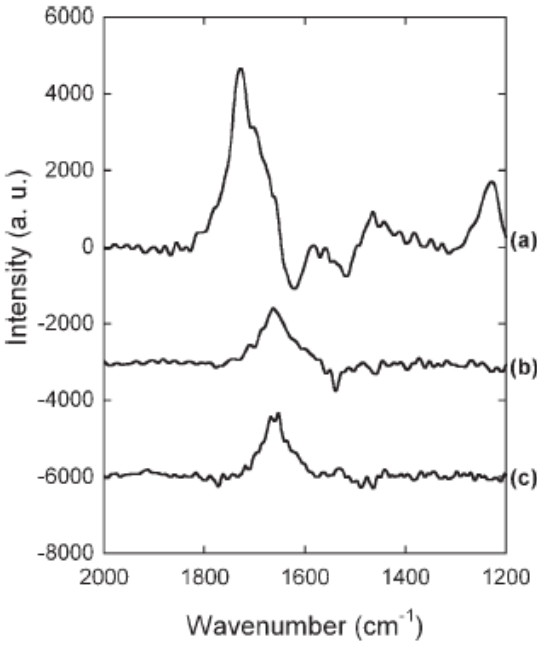

Figure 8. PM-IRRAS spectra: (a) DMPC monolayer at 40 mN/m (b) γ-gliadins (40µg) injected under a 35 mN/m DMPC monolayer (spectrum divided by that of the DMPC monolayer) (c) γ-gliadins alone injected at the air-water interface.

PM-IRRAS spectra. The γ-gliadin – DMPC monolayer system was studied by PM-IRRAS. The protein signal was very difficult to obtain, probably due to the low thickness of the aggregates and their low surface representativeness. Figure 8 displays PMIRRAS spectra of the pure DMPC monolayer (a), the ratio between the spectrum obtained after the injection of 40µl of γ-gliadins under a 35 mN/m DMPC monolayer and the DMPC spectrum (b) , and the spectrum of γ-gliadins alone at the air-water interface (c). The DMPC spectrum displays characteristic bands at 1729, 1468, 1230 cm^{-1} (fig. 8a). These bands are assigned, respectively, to the stretching of the C=O ester bonds, the CH_2 bending mode, and the antisymmetric P=O stretching vibration[41]. The γ-gliadin under the DMPC monolayer spectrum (fig. 8b) displays a band at 1665 cm^{-1} ascribed to the amide I band of the protein, and no band attributed to the DMPC monolayer. The presence of the amide band proves that proteins are not far from the air-liquid interface, whereas the absence of DMPC bands indicates that the DMPC signal is unmodified by protein adsorption and suggests thus a weak interaction between lipids and proteins. The maximum intensity of the amide I band appears at 1665 cm^{-1}, indicating a secondary structure rich in β-turns and/or small α-helices. This band appears similar to the band obtained for γ-gliadins alone injected at the air-water interface at 6300 Å²/molecule (Fig. 8b) (this molecular area roughly corresponds to a γ-gliadins injection of 2µg in the trough used for experiments made with a lipid monolayer). In both cases, the amide II band is absent. This absence can be assigned to a specific orientation of secondary structures. Our previous PM-IRRAS spectrum analysis of the γ-gliadins at the air-water interface indicates that secondary structures are flat oriented relative to the interface[16]. Considering the similarity of γ-gliadins amide bands at both air-water and DMPC-water interfaces, it can be concluded that γ-gliadins adsorbed under a DMPC monolayer is structured in β-turns and small α-helices, flat oriented relative to the phospholipidic monolayer plane.

Discussion

The 3D approach developed in this study shows that γ-gliadins can be partially inserted within a non-ionic lyotropic lamellar phase in a large range of dilutions. Whereas the bilayer thickness is constant and equal to 2.9 nm, the most confined system displays a water layer thickness of 1.8 nm. These dimensions, smaller than the dimensions of gliadin estimated in different solvants[42], suggests that gliadins inserted inside the lamellar phase adopt a thinner, and consequently more anisotropic conformation than in solution. Such an elongated conformation would be consistent with the thickness of γ-gliadin monolayers adsorbed at the air-water interface measured at low compression levels[16]. However, the dynamical study using FRAP measurements of the gliadins-lyotropic lamellar phase system also suggests additional hypotheses, stipulating that gliadin do not freely diffuse in the aqueous layer:

(1) γ-gliadins form *large* objects, soluble into water, which are geometrically confined between bilayers in the whole range of dw studied,
(2) γ-gliadins are embedded into bilayers,
(3) γ-gliadins are close to the polar head-water interface interacting with the bilayers from their water side.

The size of γ-gliadins in our system is unknown but it is important to note that gliadins can adopt very different conformations and sizes according to the nature of the solvent and the ionic strength[42]. In a good solvent, like 70% (v/v) aqueous ethanol, SAXS measurements[43] showed that the dimensions of γ-gliadins were d (diameter)=3,35nm and L(length)=12,5nm assuming a rod model. γ-gliadins can also display smaller dimensions, for example, in an acetic acid-10mM NaCl solvent, the hydrodynamic radius can be estimated to 3 nm[42].

Hypothesis (1) can be examined considering either gliadin aggregates or unfolded gliadin monomers. Taking into account the dimensions measured in a good solvent, dynamic data of gliadins in the lamellar phase can be interpreted as the result of the confined diffusion of anisotropic objects[26], which would be sterically prohibited from having their long axis parallel to the staking axis of the lamellar phase. Within the framework of hypothesis (1), however, the diffusion of confined objects is estimated to be similar to that of the same objects embedded into membranes, and current models[44,45,46] indicate that, for a given membrane system, a larger object always displays a lower diffusion coefficient than a smaller object. As a consequence, with hypothesis (1), and similarly with hypothesis (2), the protein diffusion coefficient is predicted to be smaller than for lipids embedded inside bilayers. Despite the high error bar of measurements, the reverse tendency is unambiguously observed experimentally in Fig. 4. As a further argument against hypothesis 2, transmembrane domains are not predicted in γ-gliadin sequence by the method of Zao and London [47]. That is why the hypothesis of monomeric protein close to the polar heads – water interface, interacting with the bilayers can be privileged. This interaction would induce the elongated conformation previously suggested.

In a second time, the gliadin-membrane interaction study was completed by the 2D approach using DMPC and DMPG phospholipids. Results indicate an insertion of gliadins for monolayer pressures below 20mN/m and an adsorption of gliadins under the monolayer for pressures above. Different authors, on different systems and with different experimental methods, determined bilayer-monolayer equivalence pressures in the range of 25-35mN/m[48,49,50,51]. This suggests that the equivalent pressure of bilayers in the lamellar phase is higher than 20mN/m and confirm that gliadins are in interaction with membranes, without being embedded inside them. BAM observations indicate that both γ and ω-gliadins locally adsorb under lipid monolayers to form small domains with a limited lateral expansion. This behavior suggests a nucleation-growth mechanism for the formation of gliadins aggregates under the membrane. The limited lateral growth can be attributed to an important line tension between the adsorbed gliadins aggregates and the subphase molecules in interaction with polar heads of phospholipids. The thickness of these domains was estimated by reflectivity measurements and indicated different behaviors according to the gliadin type. Initially, γ- and ω-gliadins adsorb as monolayers under the lipidic monolayer. With increasing gliadin quantity injected into the subphase, the γ-gliadins aggregate thickness grows whereas ω-gliadins aggregate thickness remains constant. Considering that γ-gliadins display an amphiphilic structure made of a hydrophobic, non-repetitive domain, and a more hydrophilic, repetitive domain, and that ω-gliadins are essentially composed of a repetitive domain, a model is proposed to explain our experimental observations (Scheme 1). The interaction between protein and membrane, observed using both γ- and ω-gliadins, could be ascribed to an interaction between polar heads of phospholipids and the repetitive domain of gliadins. This hypothesis would be in agreement with biological studies showing that the repetitive domain of gliadins is crucial for protein bodies formation in wheat [52, 53]. The exact nature of the interaction between lipids and gliadins could not be solved in our study. However, the low net charge of gliadins at the pH conditions of our experiments (γ-gliadin: +2, γ-gliadin's repetitive domain: +5, ω-gliadin: -2), and the similar observations obtained using both zwiterrionic and negatively charged monolayers exclude a predominance of electrostatic interactions. In addition, PMIRRAS measurements suggest weak gliadin-membrane interactions. Fernandez *et al*[54] showed that the extent of protein deposition on the lipid bilayer is strongly correlated with the average extent of underwrapping of backbone hydrogen bonds in the native structure of a protein. According to authors[55, 56], intramolecular hydrogen bonds that are not properly desolvated by surrounding hydrophobic groups are available to benefit from further protection by another body, like lipid bilayers, since an exogenous removal of surrounding water enhances their electrostatic stability. The extent of unprotected intramolecular hydrogen bonds is not known for gliadins, as these proteins were never crystallized. However, this content can be expected important as the primary structure of gliadin repetitive domains contains many glutamines, which are susceptible to form hydrogen bonds (47% and 43%, for γ- and ω-gliadins respectively), and few hydrophobic residues to protect intramolecular hydrogen bonds (16% and 18% for γ- and ω-gliadins respectively). Moreover, the secondary structure of wheat storage proteins repetitive domains is known to be very instable[57] and extended due to prolines and glutamines residues[58]. The proposed repetitive domain – membrane interaction could thus be explained by the protection of hydrogen bonds. Finally, the thickness growth, observed only with γ-gliadins, could be ascribed to the non-repetitive domain. A multilayer structure, characterized by a stacking of repetitive and non repetitive domains, is thus proposed. In this multilayer structure model, hydrophobic interactions are considered to be predominant in the interaction between non-repetitive domains, whereas the interaction between repetitive domains should be explained by the under-wrapped hydrogen bond model, previously described for the protein membrane interaction.

The different abilities of γ- and ω-gliadins to accumulate via an interface were previously observed at the air-water interface where gliadins form homogeneous monolayers[16]. Under lateral compression, γ-gliadins monolayer forms thicker film whereas ω-gliadins monolayer collapses. The accumulation mechanism, at the air-water interface under compression could also be due to the amphiphilic character of γ-gliadins. The interaction of gliadin with membranes was previously suggested by suction experiments on giant phospholipidic vesicles in presence of gliadins[15]. Authors interpreted the modification of mechanical properties of vesicles as an insertion of gliadins inside the bilayer.

However our results clearly indicate that γ– and ω–gliadins do not penetrate into membranes with pressure higher than the critical pressure of 20 mN/m. An insertion of gliadins in vesicle membranes can be considered only if local low pressures (<20mN/m) are induced by the suction action. Moreover, the modification of mechanical properties observed by the authors does not seem contradictory with the hypothesis of an adsorption of protein on the bilayer.

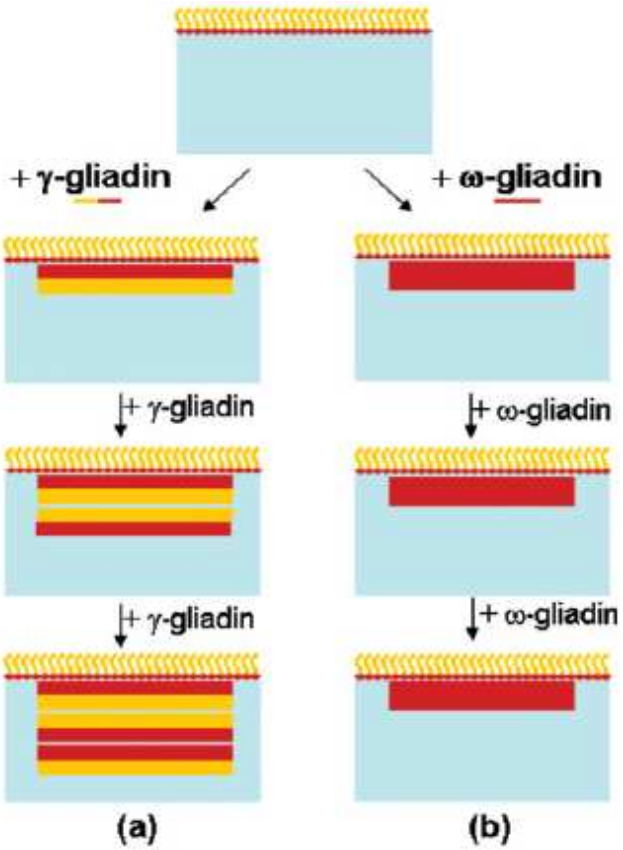

Scheme 1. Model of gliadins self-assembly via a lipidic membrane interface. (a) In the case of γ-gliadins, where the molecule is represented with the hydrophobic globular domain in yellow, and the more hydrophilic extended domain in red, the formation of a multilayer structure of γ-gliadins under the lipidic membrane would occur through mainly hydrophobic interactions. (b) In the case of ω-gliadins, where the molecule is represented in red due to its unique low hydrophobic extented domain, the formation of a ω-gliadin multilayer under the lipidic membrane would be inhibited due to the absence of hydrophobic domains within the sequence.

In summary, in this study the gliadin-membrane interaction was highlighted with two contrasting model membranes and the formation of local aggregates under the membrane was demonstrated. We propose that such processes happen in the biological context of the ER during the accumulation of prolamins in developing wheat grains. The gliadin–membrane interaction would be mediated by the repetitive domain of gliadins, and could act as a anchor for gliadins on the ER membrane and as a nucleus point for the growth of prolamin assemblies leading the protein bodies formation. The amphiphilic character of γ-gliadins would be at the origin of the accumulation process in the ER of endosperm cells.

Conclusions

The demonstration of γ- and ω-gliadins-membrane interaction, using a combined 3D approach using lamellar phases and a 2D approach using Langmuir phospholipid films, could explain the initiation of prolamins assembly within the endoplasmic reticulum of wheat endosperm cells. Moreover, the aggregate thickness growth observed in our prolamins-membrane model systems could represent a mechanism of the accumulation process occurring in the biological context. A model of accumulation process based on the amphiphilic nature of γ-gliadins is proposed. Further studies will be needed to confirm this hypothetical model of prolamins accumulation from a membrane, and in particular by better characterizing gliadin aggregates using techniques which provide local informations such as AFM and microspectroscopies.

Acknowledgments

Financial support for this work was provided by INRA and CNRS within the framework of the Groupement De Recherches Assemblages de Macromolécules Végétales (GDR AMV). We are grateful to Mr Jean-Pierre Compoint and Mrs Dominique Melcion for the purification of gliadins. We also gratefully acknowledge Prof. F. Nallet for the final manuscript correction.

References

(1) Sliwinski, E.L.; Kolster, P.; Prins, A.; van Vliet, T. J. Cereal Sci. 2004, 39, 247-264.
(2) Pallos, F.; Robertson, G.; Pavlath, A.; Orts, W. J. Agric. Food Chem. 2006, 54, 349-352.
(3) Ezpeleta, I.; Irache, J.M.; Stainmesse, S.; Chabenat, C.; Guéguen, J.; Popineau, Y.; Orecchioni, A.M. In.t J. Pharmaceutics 1996, 131, 191-200.
(4) Osborne, T.B. The vegetable proteins, 1909, Longmans, Green and Co, edited by Aders Plimmer, R.H.; Hopkins, F. G.
(5) Shewry, P. R.; Halford, N.G. Journal of Experimental Botany 2002, 53, 947-958.
(6) Tatham, A.S.; Shewry, P.R. J. Cereal Sci. 1995, 1-16.
(7) Popineau, Y. In High performance liquid chromatography of cereal and legume proteins. J.E. Kruger and J.A. Bietz, eds AACC, 1993, 393-426.
(8) Galili, G.; Shimoni, Y.; Giorini-Silfen, S.; Levanony, H. ; Alschuler, Y. ; Shani, N. Plant Physiol. Biochem. 1996, 34, 245-252.

(9) Galili, G. ; Altschuler, Y. ; Levanony, H. Trends in Cell Biology 1993, 3, 437-442.
(10) Vitale, A. ; Ceriotti, A. Plant Physiology 2004, 136, 3420-3426.
(11) Rosenberg, N. ; Shimoni, Y. ; Altschuler, Y. ; Levanony, H. ; Volokita, M. ; Galili, G. Plant Physiol. 1993, 102,61-69.
(12) Shani, N.; Rosenberg, N.; Kasarda, D.; Galili, G. The Journal of Biological Chemistry 1994, 269, 8924-8930.
(13) Altschuler, Y. ; Galili, G. J. Biol. Chem. 1994, 269, 6677-6682.
(14) Kogan, M.J. ; Lopez, O. ; Cocera, M. ; Lopez-Iglesias, C. ; de la Maza, A. ; Giralt, E. Biopolymers 2004, 73, 258-268.
(15) Monteiro, A.M.F.; Areas, E.P.G., Schröder, A., Fa, N. Colloids and Surfaces B: Biointerfaces, 2004, 34, 53-57.
(16) Banc, A. ; Desbat, B. ; Renard, D. ; Popineau, Y. ; Mangavel, C. ; Navailles, L. Langmuir, 2007, 23, 13066 - 13075.
(17) Shank, K.J. ; Su, P. ; Brglez, I. ; Boss, W.F. ; Dewey, R.E. ; Boston, R.S. Plant Physiology 2001, 126, 267-277.
(18) Egorov T.A., Odintsova T.I., Musolyamov A.K., Barbashov S.F., Pustobaev V.N., Anfersen J., Roepstorff P., Popineau Y. Biochemistry (Moscow) 1998, 63, 1061-1067.
(19) Piston F., Dorado G., Martin A., Barro F. J. Cereal Sci. 2006, 43, 120-128.
(20) DuPont FM., Vensel WH, Chan R., Kasarda DD. Cereal Chem. 2000, 55, 607-614.
(21) Hsia C.C., Anderson O.D. Theor. Appl. Genet. 2001, 103, 37-44.
(22) Hassani M.E., Shariflou M.R., Gianibelli M.C., Sharp P.J J. Cereal Sci. 2008, 47, 59-67.
(23) Jonströmer, M.; Strey, R. J. Phys. Chem.1992, 96, 5993-6000.
(24) Freyssingeas, E.; Nallet, F.; Roux, D. Langmuir 1996, 12, 6028-6035.
(25) Seiffert, S.; Oppermann, W. Journal of Microscopy 2005, 220, 20-30.
(26) Moreau, P. ; van Effenterre, D. ; Navailles, L.; Nallet, F. ; Roux, D. Eur. Phys. J. E 2008 26, 225–234.
(27) Blaudez, D.; Turlet, J. M.; Dufourcq, J.; Bard, D.; Buffeteau, T.; Desbat, B. J. Chem. Soc. Faraday Trans. 1996, 92 (4), 525-530.
(28) P.G. de Gennes, The Physics of Liquid Crystal, 1993, Clarendon Press, Oxford.
(29) Faxén, H. Ann. Phys. 1922, 89, 119, quoted from J. Happel, B. Brenner, in Low Reynolds number hydrodynamics (Kluwer Academic Publishers Group, Dordrecht, 1983)
(30) Karolin, J.; Geddes, C. D.; Wynne, K.; Birch, D. J. S. Meas. Sci. Technol. 2002, 13, 21-27.
(31) Eichler, H. J.; Klein, U. K. A.; Langhans, D. Chem. Phys. Lett. 1979, 67, 21-23.
(32) Olivini, F.; Beretta, S.; Chirico, G. Appl. Opt. 2001, 55, 311-317.
(33) Keller, R. C. A.; Orsel, R.; Hamer, R.J. Journal of Cereal Sci. 1997, 175-183.
(34) Maget-Dana, R. Biochimica Biophysica Acta 1999, 1462, 109-140.
(35) Casas, J.; Espina, M.; Haro, M.; Royo, F.; Alsina, M. A.; Haro, I.; Mestres, C. Langmuir 2006, 22, 246-254.
(36) Maltseva, E.; Kerth, A.; Blume, A.; Mohwald, H. and Brezesinski, G. ChemBioChem 2005, 6, 1817-1824.
(37) Rakotomanga, M., Loiseau, P.M. ; Saint-Pierre-Chazalet, M. Biochimica Biophysica Acta 2004, 1661, 212-218.
(38) Buffeteau, T.; Desbat, B. Applied Spectroscopy 1989, 43, 1027-1032.
(39) Winsel, K. ; Honing, D. ; Lunkenheimer, K. ; Geggel, K. ; Witt, C. Eur. Biophys J. 2003, 32, 544-552.
(40) Brechling, A.; Pohl, M.; Kleinberg, U.; Heinzmann, U. Journal of Biotechnology 2004, 112, 115-125.
(41) Cornut, I. ; Desbat, B. ; Turlet, J. M. ; Dufourcq, J. Biophys. J. 1996, 70, 305-312.
(42) data calculated from Popineau, Y; and Pineau, F. Lebensm. Wiss. U. Technol. 1988, 21, 113-117.
(43) Thomson, N.H., Miles, M.J., Popineau, Y., Harries, J., Shewry, P.R., Tatham, A.S. Biochim Biophys. Acta 1999, 1430, 359-366.
(44) Saffman, P.G.; Delbrück, M. Proc. Nat. Acad. Sci USA 1975, 72, 3111-3113.
(45) Naji, A.; Levine, A. J.; Pincus, P. A. Biophys. J. 2007, 93, 49-51.
(46) Gambin, Y.; Lopez-Esparza, R.; Reffay, M. ; Sierecki, E. ; Gov, N.S. ; Genest, M.; Hodges, R. S.; Urbach, W. Proc. Natl. Acad. Sci. USA 2005, 103, 2098-2102.
(47) Zhao, G. ; London, E. Protein Science, 2006, 15, 1987-2001.
(48)Annette Meister, Andreas Kerth, and Alfred Blume, *J. Phys. Chem. B* 2004, *108*, 8371-8378.
(49) Seelig, A. *Biochim. Biophys. Acta* 1987, *899*, 196-204; Blume, A. *Biochim. Biophys. Acta* 1979, *557*, 32-44.
(50)Schindler, H. *Biochim. Biophys. Acta* 1979, *555*, 316-336.
(51) Demel, R. A.; Geurts van Kessel, W. S. M.; Zwaal, R. F. A.;Roelofsen, B.; Van Deenen, L. L. M. *Biochim. Biophys. Acta* 1975, *406*, 97-107.
(52) Rosenberg, N.; Shimoni, Y.; Altschuler, Y.; Levanony, H.; Volokita, M. and Galili, G. Plant Physiol. 1993, 102, 61-69.
(53) Altschuler, Y.; Rosenberg, N. ; Harel, R. and Galili, G. The Plant Cell 1993, 5, 443-450.
(54) Fernandez, A.; Berry, R. S. Proc. Nat. Acad. Sci USA 2003, 100, 2391-2396.
(55) Fernandez, A.; Scheraga, H. A. Proc. Nat. Acad. Sci USA 2003, 100, 113-118.
(56) Fernandez, A. Journal of Chemical Physics 2003, 119, 6911-6915.
(57) Tatham, A.S. ; Masson, P. ; Popineau, Y. J. Cereal Sci. 1990, 11, 1-3.
(58) Masci, S.; D'Ovidio, R.; Lafiandra, D.; Kasarda, D. D. Plant Physiol. 1998, 118, 1147-1158.